Received: 8 April 2021 | Revised: 23 May 2021 | Accepted: 4 June 2021

DOI: 10.1049/mia2.12174

IET Microwaves, Antennas & Propagation

The Institution of Engineering and Technology WILEY

ORIGINAL RESEARCH PAPER

Coupling effects in array-fed reflector antennas with digital beamforming

Sigurd Huber[1] | Su Yee Aye[2] | Koenraad Mouthaan[2] | Gerhard Krieger[1]

[1]Microwaves and Radar Institute, German Aerospace Center (DLR), Oberpfaffenhofen, Germany

[2]Faculty of Engineering, National University of Singapore (NUS), Singapore

Correspondence

Sigurd Huber, Microwaves and Radar Institute, German Aerospace Center (DLR), Oberpfaffenhofen, Germany.
Email: sigurd.huber@dlr.de

Abstract

Many modern microwave systems, for example, in the field of satellite communications, remote sensing for Earth observation or radio astronomy, employ reflector antennas with beam-shaping capabilities. A generalised description of multi-channel receiver architectures with digital beamforming, employing scattering parameter formalism is presented here. Special emphasis has been placed on noise modelling, where noise sources have been included also at the input ports of the receive amplifiers. The performance of such a system is evaluated in terms of the signal-to-noise ratio (SNR) and the signal-to-interference ratio at the beamformer output. The basis for this analysis is a design example of a reflector antenna fed by a linear patch array, whose *S*-parameters have been computed by means of electromagnetic simulations. In this work, two scenarios are addressed. In the first case, the effect of coupling has been neglected in the derivation of the beamforming weights. The main consequence appears to be a severely impaired interference suppression performance. In the second scenario, which has not been addressed in the literature so far, noise from the input ports of the receive amplifiers couple via the antenna radiators and can result in a loss of SNR at the beamformer output if neglected in the beamforming process.

1 | INTRODUCTION

Exchange and retrieval of information using electromagnetic (EM) waves has found ever-increasing fields of application in commerce, science, military or civil services. One example is communications employing satellites, but there are also several other fields, where information retrieval via microwaves has proven indispensable. For instance, spaceborne Earth observation [1–3] is an application in the field of remote sensing, where radar pulses are sent to ground and their echoes are recorded by the radar satellite. Another area of great scientific importance is radio astronomy [4], in which interesting signals from deep space are collected using radio telescopes.

A technological commonality between these areas of application is that they heavily rely on systems employing large reflector antennas. The motivation for this is obvious. Usually the distances between the communication participants, or even more so the distance between the origin of deep space signals and receivers on Earth, is large. Therefore, a highly directive antenna shall guarantee enough sensitivity to detect useful signals in a background of clutter and noise.

Considering the increasing number of microwave systems, as for example, communications satellites, they are not only disturbed by natural noise but also interfere with each other. Traditionally, mutual interference has been combatted by separating information exchange in time and frequency. However, in recent years, innovative antenna architectures using multiple receive channels allowed exploring the spatial domain in order to isolate information against interferences. With the so-called digital beamforming systems [4–10], it is possible to amplify a signal of interest by pointing a high gain beam towards its direction and, at the same time, suppress unwanted interferers originating from other directions. However, coupling, which may occur in a multi-channel receiver environment, can pose serious challenges. Several publications address the problem of coupling, for instance, for communication systems [11–14]. However, little attention has been paid to noise modelling in multi-channel receiver

architectures. Generally, if neglected or not properly taken into account in the beamforming algorithms, coupling can result in a loss of sensitivity and interference suppression capability.

This work aims to provide a better understanding of the EM behaviour of array-fed reflector-based digital beamforming systems in the presence of coupling and represents an extension and generalisation of analysis which has been carried out, for example, in [15–17]. In particular, the effect of noise coupling in array-fed reflector-based systems is investigated. For this, a network theoretical model has been established (Section 2), which allows simulating EM coupling in the antenna system up to the digitisation stage of the signals. A dedicated L-band example of an array-fed reflector antenna in the size-class of Tandem-L [3] has been designed (Section 3). Evaluating this design in terms of the *S*-parameters (Section 4), enabled us to simulate digital beamforming (Section 5) with special emphasis on a null-steering technique for interference rejection. The paper concludes with a discussion of the main findings (Section 6).

2 | A NETWORK MODEL FOR MULTI-CHANNEL ANTENNA SYSTEMS

Treating an antenna system with all its components, for example, the antenna structure itself, amplifiers or filters, by pure EM field simulations is highly complicated and computationally very demanding. An advantage of modern EM software is that it can take network parameters, in particular *S*-parameters, as input or deliver them as a result of EM simulations. This allows for a computationally efficient, yet accurate treatment of complex antenna architectures.

Of major importance is of course the antenna structure including the reflector, feed radiators as well as the feed distribution network. From a modelling perspective, the antenna represents the interface between EM fields and network quantities. For the purpose of theoretical treatment and for practical antenna measurements, a model described by the so-called *source scattering-matrix equations* has been established [18–20]. The defining equations, describing an antenna with a single port, are

$$b_{0,i_1\cdots i_N} := \sum_{j_1\cdots j_M} S^{j_1\cdots j_M}_{i_1\cdots i_N} a_{0,j_1\cdots j_M} + T_{i_1\cdots i_N} a_1, \tag{1}$$

$$b_1 := \sum_{j_1\cdots j_M} R^{j_1\cdots j_M} a_{0,j_1\cdots j_M} + \Gamma a_1 \tag{2}$$

and they obey Maxwell's equations under the assumption of a linear medium. The first set of equations represents outgoing waves at the antenna-air interface (cf. left part of Figure 1), where the $b_{0,i_1\cdots i_N}$ represent the total field composed of the scattered field (the sum-terms with S) and the transmitted field (the terms with T). The second equation describes the antenna in the receive mode. b_1 is the incoming wave as superposition of the received field (the sum-terms with R) and the input reflection (the term with Γ) at the antenna port. The various indices may refer to different decompositions of the fields. For example, Kerns [18] uses two indices denoting different field regions and polarisations. He interprets the quantities T and R as the 'transmitting' and 'receiving characteristics'. In [19, 20], the indices refer to modal coefficients as used in *multipole expansions*. Being omitted here, Equations (1) and (2) depend of course on some variables. Here, we will use frequency f and a single angle ϑ, which is sufficient for far field considerations.

In the following, we adapt the source scattering-matrix equations such that they describe multi-channel antennas. First, one has to notice that in (2), the in and outgoing waves (a_1, b_1) at the antenna port become vector quantities $(\boldsymbol{a}_1, \boldsymbol{b}_1)$ with N components, each representing a channel. Moreover, the terms with T and R shall be interpreted as *embedded patterns*, while the terms with S and Γ represent the scattering characteristics of the antenna. In order to use vector-matrix notation, we discretise the angular coordinate with M directions. Lewis [19] uses 'infinite-dimension' column, row and square matrices. Incidentally, this is the same description used for the so-called MIMO systems in communications [15]. This allows expressing the entire antenna system in terms of network equations (see also [21])

$$\begin{pmatrix} \boldsymbol{b}_0 \\ \boldsymbol{b}_1 \end{pmatrix} = \begin{pmatrix} \boldsymbol{S}_{00} & \boldsymbol{S}_{01} \\ \boldsymbol{S}_{10} & \boldsymbol{S}_{11} \end{pmatrix} \begin{pmatrix} \boldsymbol{a}_0 \\ \boldsymbol{a}_1 \end{pmatrix} + \begin{pmatrix} \boldsymbol{n}_0 \\ \boldsymbol{n}_1 \end{pmatrix}, \quad \boldsymbol{S}_{01}\boldsymbol{a}_1 \approx \boldsymbol{0}, \tag{3}$$

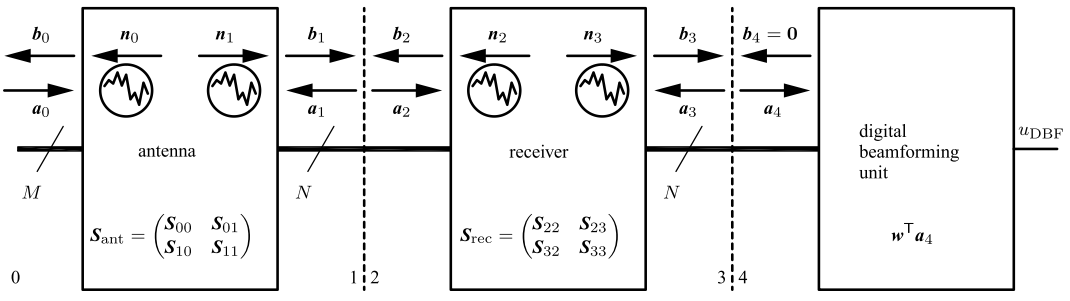

FIGURE 1 Network model representing a multi-channel antenna system. M plane waves enter an antenna with N receive channels. In the digital beamforming unit, a single data stream is formed out of the N signals $\boldsymbol{a}_4$. The subscript numbers refer to the interfaces written at the bottom of the block diagram

$$\begin{pmatrix} \boldsymbol{b}_2 \\ \boldsymbol{b}_3 \end{pmatrix} = \begin{pmatrix} \boldsymbol{S}_{22} & \boldsymbol{S}_{23} \\ \boldsymbol{S}_{32} & \boldsymbol{S}_{33} \end{pmatrix} \begin{pmatrix} \boldsymbol{a}_2 \\ \boldsymbol{a}_3 \end{pmatrix} + \begin{pmatrix} \boldsymbol{n}_2 \\ \boldsymbol{n}_3 \end{pmatrix}, \tag{4}$$

$$\boldsymbol{b}_1 = \boldsymbol{a}_2, \quad \boldsymbol{b}_2 = \boldsymbol{a}_1, \quad \boldsymbol{b}_3 = \boldsymbol{a}_4, \quad \boldsymbol{b}_4 = \boldsymbol{a}_3 \approx \boldsymbol{0}, \tag{5}$$

where Equations (1) and (2) have been combined into (3). It is important to mention here that these equations are Fourier domain representations and therefore depend on frequency f. The corresponding block diagram is provided in Figure 1, showing the components of the antenna system, including the antenna ($\boldsymbol{S}_{\text{ant}}$), the receive chain ($\boldsymbol{S}_{\text{rec}}$) and the digital beamforming unit. The receive chain typically contains the low noise amplifiers. At interface 1 and 2, we do not impose a dedicated matching network and simply assume the receiver hardware to be matched to the antenna, which requires $\boldsymbol{S}_{22} = \boldsymbol{S}_{11}^{\mathsf{H}}$. Here, superscript H denotes conjugate transpose. The final output is a single signal u_{DBF}, which is formed by a proper selection of weights $\boldsymbol{w}$ applied to the beamformer input signals $\boldsymbol{a}_4$. The discussion in this paper is based on a single polarisation. However, an extension to a dual polarised antenna is straightforward. Interested readers are directed to refer the Appendix.

Special focus in this work is on thermal noise and its propagation through the system. For this, several *internal noise sources* $\boldsymbol{n}$ have been introduced, generalising the analysis given for example in [17]. In this context, the internal noise sources $\boldsymbol{n}_1$ at the antenna output ports might be understood as superposition of external brightness temperature captured by the antenna and thermal noise generated in the antenna structure itself.

A first elimination of Equations 3–5 gives

$$\boldsymbol{b}_2 = \boldsymbol{S}_{22}(\boldsymbol{S}_{10}\boldsymbol{a}_0 + \boldsymbol{S}_{11}\boldsymbol{b}_2 + \boldsymbol{n}_1) + \boldsymbol{n}_2, \tag{6}$$

$$\boldsymbol{a}_4 = \boldsymbol{S}_{32}(\boldsymbol{S}_{10}\boldsymbol{a}_0 + \boldsymbol{S}_{11}\boldsymbol{b}_2 + \boldsymbol{n}_1) + \boldsymbol{n}_3. \tag{7}$$

Equation (6) solved for $\boldsymbol{b}_2$ and inserted into (7) finally yields the input signal at the beamforming stage

$$\boldsymbol{a}_4 = \boldsymbol{A}\boldsymbol{a}_0 + \boldsymbol{B}\boldsymbol{n}_1 + \boldsymbol{C}\boldsymbol{n}_2 + \boldsymbol{n}_3, \tag{8}$$

where

$$\boldsymbol{A} = \boldsymbol{S}_{32}(\mathbf{I} - \boldsymbol{S}_{11}\boldsymbol{S}_{22})^{-1}\boldsymbol{S}_{10}, \quad \in \mathbb{C}^{N\times M} \tag{9}$$

$$\boldsymbol{B} = \boldsymbol{S}_{32}(\mathbf{I} - \boldsymbol{S}_{11}\boldsymbol{S}_{22})^{-1}, \quad \in \mathbb{C}^{N\times N} \tag{10}$$

$$\boldsymbol{C} = \boldsymbol{S}_{32}\boldsymbol{S}_{11}(\mathbf{I} - \boldsymbol{S}_{11}\boldsymbol{S}_{22})^{-1}, \quad \in \mathbb{C}^{N\times N} \tag{11}$$

and $\mathbf{I}$ represents the identity matrix. Here, the symmetry of the matrices $\boldsymbol{S}_{11}$ and $\boldsymbol{S}_{22}$ has been exploited yielding $\mathbf{I} + \boldsymbol{S}_{11}(\mathbf{I} - \boldsymbol{S}_{22}\boldsymbol{S}_{11})^{-1}\boldsymbol{S}_{22} = (\mathbf{I} - \boldsymbol{S}_{11}\boldsymbol{S}_{22})^{-1}$. A proper choice of the beamforming coefficients $\boldsymbol{w}$ requires first the computation of the power contained in the beamformer output signal

$$\begin{aligned} P_{u_{\text{DBF}}} &= \mathcal{E}\{|u_{\text{DBF}}|^2\} = \mathcal{E}\{|\boldsymbol{w}^{\mathsf{T}}\boldsymbol{a}_4|^2\} \\ &= \boldsymbol{w}^{\mathsf{T}}\mathcal{E}\{\boldsymbol{a}_4\boldsymbol{a}_4^{\mathsf{H}}\}\boldsymbol{w}^* = \boldsymbol{w}^{\mathsf{T}}\boldsymbol{R}\boldsymbol{w}^*, \end{aligned} \tag{12}$$

with the covariance matrix

$$\begin{aligned} \boldsymbol{R} = &\underbrace{\boldsymbol{A}\mathcal{E}\{\boldsymbol{a}_0\boldsymbol{a}_0^{\mathsf{H}}\}\boldsymbol{A}^{\mathsf{H}}}_{\boldsymbol{R}_{\text{s+i}}} \\ &+ \underbrace{\boldsymbol{B}\mathcal{E}\{\boldsymbol{n}_1\boldsymbol{n}_1^{\mathsf{H}}\}\boldsymbol{B}^{\mathsf{H}} + \boldsymbol{C}\mathcal{E}\{\boldsymbol{n}_2\boldsymbol{n}_2^{\mathsf{H}}\}\boldsymbol{C}^{\mathsf{H}} + \mathcal{E}\{\boldsymbol{n}_3\boldsymbol{n}_3^{\mathsf{H}}\}}_{\boldsymbol{R}_{\text{n}}}, \end{aligned} \tag{13}$$

where the symbol $\mathcal{E}$ denotes expectation. The first term in Equation (13) refers to signal plus interference, while the last three terms describe mutually independent noise. In principle, the noise sources $\boldsymbol{n}_2$ and $\boldsymbol{n}_3$ could be correlated, in which case another two noise covariance terms $\boldsymbol{C}\mathcal{E}\{\boldsymbol{n}_2\boldsymbol{n}_3^{\mathsf{H}}\}$ and $\mathcal{E}\{\boldsymbol{n}_3\boldsymbol{n}_2^{\mathsf{H}}\}\boldsymbol{C}^{\mathsf{H}}$ would appear.

For example, in a spaceborne Earth observation system, interference could be unwanted echoes from preceeding or succeeding radar echoes, called as range ambiguities. In communication systems, typically inter-satellite interference may occur or interference from ground signals. Receivers for radio astronomy can suffer from spillover into their frequency band. Assuming that these interferers are spatially separated from the signal direction, an optimisation problem

$$\text{minimize} \qquad \boldsymbol{w}^{\mathsf{T}}\boldsymbol{R}_{\text{n}}\boldsymbol{w}^* \tag{14}$$

$$\text{subject to} \qquad \boldsymbol{A}^{\mathsf{T}}\boldsymbol{w} = \boldsymbol{c} \tag{15}$$

can be formulated where a constraint vector $\boldsymbol{c}$ is introduced. This vector could contain a '1' corresponding to the signal of interest (direction ϑ_0) and zeros for the $M-1$ interferer directions (ϑ_i) to be suppressed. This optimisation problem has an analytic solution

$$\boldsymbol{w}^* = \boldsymbol{R}_{\text{n}}^{-1}\boldsymbol{A}(\boldsymbol{A}^{\mathsf{H}}\boldsymbol{R}_{\text{n}}^{-1}\boldsymbol{A})^{-1}\boldsymbol{c}^*, \tag{16}$$

known as *linear constrained minimum variance* (LCMV) beamformer [22].

Let signal and interference be decomposed according to

$$\boldsymbol{a}_0 = \boldsymbol{a}_{0\text{s}} + \boldsymbol{a}_{0\text{i}}, \tag{17}$$

Then, the signal-plus-interference covariance matrix $\boldsymbol{R}_{\text{s+i}}$ in Equation (13) can be split into a signal- and interference-only covariance matrix

$$\boldsymbol{R}_{\text{s}} = \boldsymbol{A}\mathcal{E}\{\boldsymbol{a}_{0\text{s}}\boldsymbol{a}_{0\text{s}}^{\mathsf{H}}\}\boldsymbol{A}^{\mathsf{H}}, \tag{18}$$

$$\boldsymbol{R}_{\text{i}} = \boldsymbol{A}\mathcal{E}\{\boldsymbol{a}_{0\text{i}}\boldsymbol{a}_{0\text{i}}^{\mathsf{H}}\}\boldsymbol{A}^{\mathsf{H}}, \tag{19}$$

assuming that signal and interference differ in their direction of arrival. For the purpose of performance evaluation, this allows us to define the signal-to-noise ratio (SNR), the signal-to-

interference ratio (SIR) and the signal-to-interference-plus-noise ratio (SINR)

$$\mathrm{SNR}(\vartheta): = \frac{\int_f \boldsymbol{w}^{\mathsf{T}} \boldsymbol{R}_{\mathrm{s}}(\vartheta)\boldsymbol{w}^{*}\mathrm{d}f}{\int_f \boldsymbol{w}^{\mathsf{T}} \boldsymbol{R}_{\mathrm{n}}\boldsymbol{w}^{*}\mathrm{d}f}, \tag{20}$$

$$\mathrm{SIR}(\vartheta_0): = \frac{\int_f \boldsymbol{w}^{\mathsf{T}} \boldsymbol{R}_{\mathrm{s}}(\vartheta_0)\boldsymbol{w}^{*}\mathrm{d}f}{\int_f \boldsymbol{w}^{\mathsf{T}} \boldsymbol{R}_{\mathrm{i}}\boldsymbol{w}^{*}\mathrm{d}f}, \tag{21}$$

$$\mathrm{SINR}(\vartheta_0): = \frac{\int_f \boldsymbol{w}^{\mathsf{T}} \boldsymbol{R}_{\mathrm{s}}(\vartheta_0)\boldsymbol{w}^{*}\mathrm{d}f}{\int_f \boldsymbol{w}^{\mathsf{T}} (\boldsymbol{R}_{\mathrm{i}} + \boldsymbol{R}_{\mathrm{n}})\boldsymbol{w}^{*}\mathrm{d}f}. \tag{22}$$

3 | ARRAY-FED REFLECTOR DESIGN EXAMPLE

To demonstrate the impact of coupling in a digital beamforming system, a spaceborne Earth observation scenario [3] has been taken as the base. The radar sensor employs an array-fed reflector as shown in Figure 2 with a multi-channel receiver architecture. The antenna has been simulated at L-band over a bandwidth of 150 MHz centred on a frequency of 1.2575 GHz (wavelength $\lambda_{\mathrm{c}} = 23.84$ cm). The parabolic reflector has a circular aperture with a diameter D of 15 m, a focal length F of 13.5 m and is offset O by 7.5 m. The feed array is centred on the focal point and tilted to the reflector centre for optimal illumination by an angle ψ of 31.4°. Connected to the feed array is the multi-channel receiver as shown in Figure 1. The reflector and feed array assembly is depicted here in its orientation in space where the feed array would be aligned horizontally and signal and interference would represent echoes from the Earth surface.

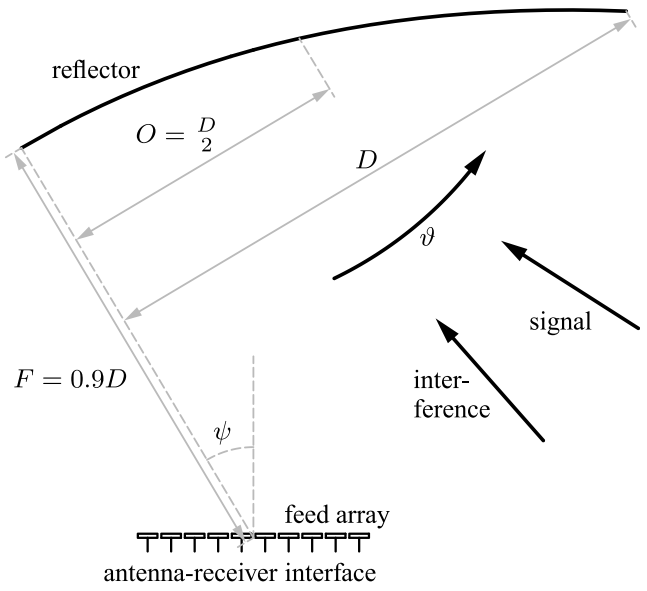

FIGURE 2 Array-fed offset reflector as it would be oriented in a spaceborne Earth observation scenario, where the feed array is aligned horizontally. Signal and interference are radar echoes from the Earth surface. Below the feed array is the interface to the multi-channel receiver

A graphical illustration of the linear feed array is presented in Figure 3. It consists of 10 rectangular patches, which are equally spaced by $\Delta L = 0.7\ \lambda_{\mathrm{c}}$. The choice of the spacing represents a compromise between the capability to form beams in each direction of interest without gain loss, if the spacing were too large; a design with reasonable coupling, if the spacing were too small, and, at the same time, the potential to have sufficient degrees of freedom during beamforming. The feed pins, indicated by black dots, have a radius of 0.275 cm and a length of 2 cm, which is the distance between the patches and the ground plane. The patches are offset to the patch centre by a distance o of 4.26 cm. During the design process, the following patch dimensions have been found optimal: The lengths L_i equal 10.61 cm for Patch #1, 10.70 cm for Patches #2–#9 and 10.60 cm for Patch #10. The widths W_i equal 10.59 cm for Patch #1, 10.56 cm for Patches #2–#9 and 10.60 cm for Patch #10.

4 | EM SIMULATIONS AND *S*-PARAMETERS

The EM simulation of the array-fed reflector antenna has been performed in Ansys HFSS, Electromagnetic Suite version 18.2. First, the feed array design has been optimised without the reflector. The feed pins have been assigned as 'perfect electric conductor' (PEC). Since 'PEC' cannot be assigned to surfaces, 'perfect E' boundaries have been assigned instead to the surfaces of the patches and the ground plane. 'Perfect E' represents a perfectly conducting surface and has the same electrical property as 'PEC'. To excite the patches, 'lumped ports' have been applied at the edges of the pins. Lumped ports are two terminal excitations with one terminal on the pin and the other terminal on the ground plane. At each port, a 50-Ω port impedance has been specified with an incident voltage of 1 V. A hybrid finite element-boundary integral (FE-BI) boundary condition has been assigned to the radiation box of the feed array, so that the feed-array inside could be solved with the finite element method (FEM), while the boundary surface has been solved with an integral equation (IE) approach. Generally, with the FE-BI approach, small bounded objects are individually solved inside using a FEM solver, while interactions with objects located at electrically large distances in unbounded space are solved with an IE solver. Hence, the FE-BI technique allows a traditional FEM solver to be efficiently applied

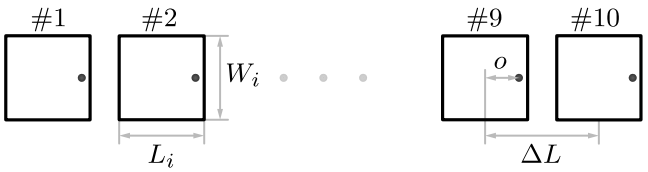

FIGURE 3 Linear feed array with 10 rectangular patches simulated on a ground plane

for large open problems with reduced computational load. In our design, the feed array is an object, bounded by a FE-BI boundary, so that later the interaction with the reflector can be simulated efficiently. The feed arrays have been designed to have low reflection coefficients in the frequency band of 150 MHz around the centre frequency. Combined with the feed array design, the offset reflector antenna has been simulated with a 'perfect E' boundary assigned to it.

For comparison, the magnitudes of the scattering parameters $\boldsymbol{S}_{11}$ for the feed array without reflector are shown in Figure 4a, while the scattering magnitudes for the entire feed-array-reflector assembly are presented in Figure 4b. It can be observed that mutual coupling between adjacent elements $(i, i+1)$ and $(i+1, i)$, $i \in [1, ..., 9]$, respectively, is quite strong, which can be explained by the polarisation of the feed array.

A direct comparison of the coupling parameter $S_{11,12}$[1] of the array-fed reflector and the feed array alone is presented in Figure 5. The ripple in the array-fed reflector case is a consequence of EM coupling between feed array and reflector. The condition for the local minima is that the coupling path length r must approximately be equal to an integer multiple (k) of a wavelength λ_k

$$r \approx (2k+1)\lambda_k. \tag{23}$$

Estimating r for the given reflector-feed design to be in the order of 29 m, this results in k discrete frequencies

$$f_k \approx \frac{2k+1}{2r}c, \quad k \in [115, \ldots, 128]. \tag{24}$$

In Figure 5, these frequencies are indicated by the vertical dashed lines and although amplitude effects have been neglected, they show a remarkable agreement with the periodicity of the ripple on the coupling parameter.

5 | BEAMFORMING ANALYSIS

Based on these *S*-parameter simulations, the beamforming performance of the array-fed reflector is investigated in terms of the SNR, the SIR and the SINR. With respect to the application, we have an Earth observation scenario in mind. Here, the suppression of interference, caused for instance by the nadir echoes, which can be quite strong compared with the signal of interest, is essential for the imaging performance. Another source of interference in quad-polarisation imaging are co-polar range ambiguities contaminating the cross-polar signal and therefore require deep nulling in the sidelobes. In such situations, coupling can lead to noticeable performance degradation if not taken into account properly. Regarding the sensitivity of such systems, even small losses in the SNR

[1]As reminder: '11' refers to sub-matrix 11 of $\boldsymbol{S}_{\text{ant}}$ (see Figure 1) and '12' denotes the element in the first row, second column of that sub-matrix.

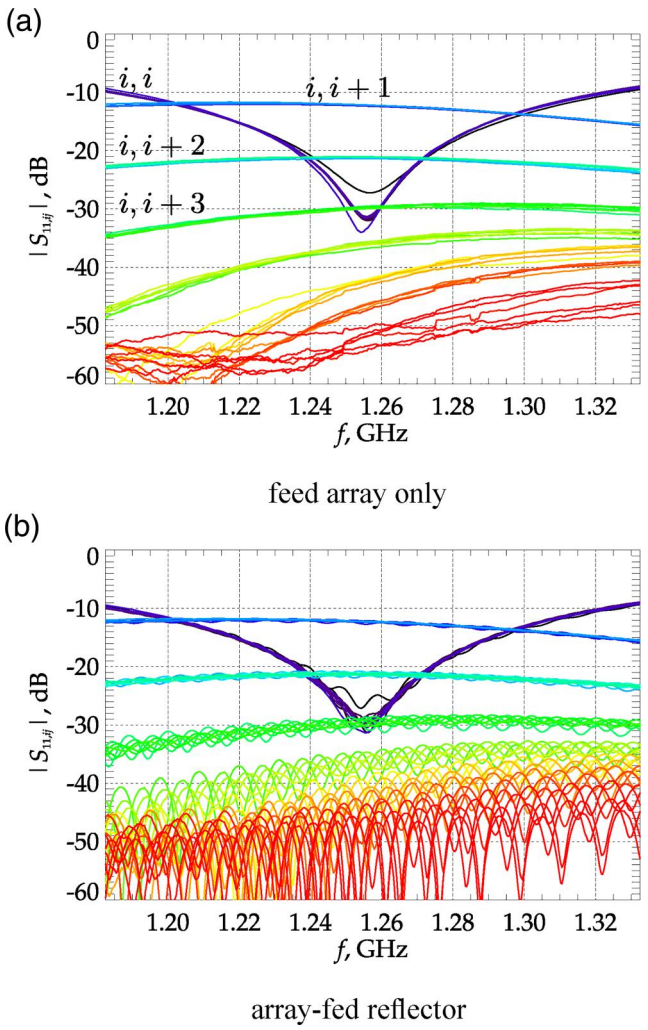

FIGURE 4 Magnitude of the antenna scattering parameters $\boldsymbol{S}_{11}$ considering the feed array without reflector (a) and the case when the feed array faces a reflector (b). Here, i is a count index for the feed elements. For instance, i, $i+1$ with $i = 5$ indicates coupling between element five and six

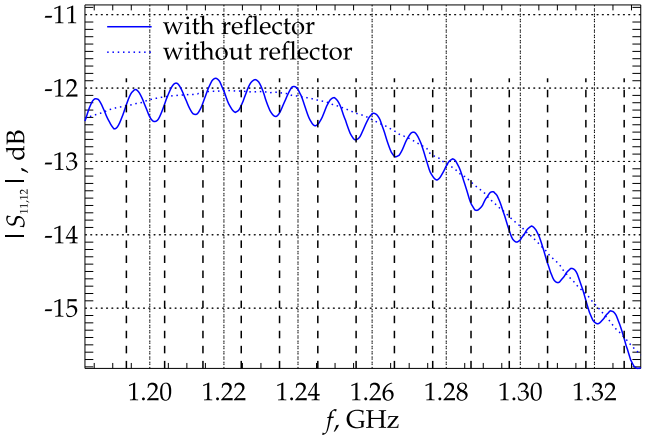

FIGURE 5 Comparison of the coupling parameter $S_{11,12}$ with and without reflector. The vertical dashed lines indicate frequencies with destructive interference according to Equation (24)

matter, because due to the large swath width and fine resolution typically required, transmit power is a costly resource.

One key question to be addressed here is, how a beamformer, in particular the LCMV beamformer, responds if coupling is neglected. Moreover, the impact of the thermal noise sources $\boldsymbol{n}_2$ (see Figure 1) [17, 23, 24] on the beamformer output shall be investigated, since they are typically neglected in the system modelling.

For a meaningful comparison, we define a reference case, which assumes perfect knowledge of all terms in the beamforming weight vector (16), namely the noise covariance matrix (see Equation 13) and the embedded antenna patterns $\boldsymbol{A}$ according to Equation (9). A performance comparison against this reference case shall uncover any degradations for imprecisely characterised systems. At this point, we also have to make assumptions about the various quantities involved. Signal, interference as well as noise shall be modelled as mutually uncorrelated, circular complex, Gaussian processes with zero mean and non-vanishing variance. For the receiver architecture assumed here, the relation between the variances (powers) of the noise sources $\boldsymbol{n}_1$ and $\boldsymbol{n}_3$ may be found from

$$\frac{\sigma^2_{\boldsymbol{n}_3}}{\sigma^2_{\boldsymbol{n}_1}} = G\frac{T_0}{T_{\text{ant}}}(F-1), \tag{25}$$

where G is the LNA gain (the square of the diagonal elements of $\boldsymbol{S}_{32}$), T_0 is the standard temperature (290 K), T_{ant} is the brightness temperature received by the antenna and F represents the system noise figure. Since we are assuming an Earth observation scenario, the antenna brightness temperature roughly equals the standard temperature. With an LNA gain of 30 dB and a system noise figure of 3 dB, the variances of noise sources $\boldsymbol{n}_1$ would be 30 dB lower than those of the noise terms $\boldsymbol{n}_3$. It is clear that these values strongly depend on the system under consideration. Even more difficult to estimate is the power contained in the noise sources $\boldsymbol{n}_2$. Here, we assume the variances $\sigma^2_{\boldsymbol{n}_2}$ to be 50 dB below the variances of $\boldsymbol{n}_3$, which could be a rather optimistic case. Moreover, coupling shall only occur at antenna level, for example, the receiver scattering matrix $\boldsymbol{S}_{32}$ is taken as identity matrix times the square root of G. This assumption is probably justified, since most of the energy couples via the feed-radiators. Regarding signal and interference, a scenario is assumed where the signal and interference variances, $\sigma^2_{\boldsymbol{a}_{0\text{s}}}$ and $\sigma^2_{\boldsymbol{a}_{0\text{i}}}$, lie 50 and 30 dB below the noise power variances $\sigma^2_{\boldsymbol{n}_3}$, respectively, which means that the interferer is 20 dB stronger compared with the signal. This could occur, for instance, if a range ambiguity originating from a bright target, like a city, would overlay the radar echo from a weakly back-radiating surface, like a water surface. Another example are the above-mentioned nadir returns, which are usually much stronger than the signal of interest. Table 1 summarises all relevant simulation parameters including the constraint vector $\boldsymbol{c}$ in Equation (16).

In practice, one might neither have complete knowledge of the coupling in the system, nor a precise noise characterisation. For our comparison, this means substituting the identity matrix

TABLE 1 Performance parameters

$\sigma^2_{\boldsymbol{a}_{0\text{s}}}/\sigma^2_{\boldsymbol{n}_3}$	−50 dB	G	30 dB
$\sigma^2_{\boldsymbol{a}_{0\text{i}}}/\sigma^2_{\boldsymbol{n}_3}$	−30 dB	F	3 dB
$\sigma^2_{\boldsymbol{n}_1}/\sigma^2_{\boldsymbol{n}_3}$	−30 dB	T_0/T_{ant}	1
$\sigma^2_{\boldsymbol{n}_2}/\sigma^2_{\boldsymbol{n}_3}$	−50 dB	$\boldsymbol{c}^{\text{T}}$	$\begin{pmatrix}1 & 10^{-3}\end{pmatrix}$

$\mathbf{I}$ for the noise covariance matrix $\boldsymbol{R}_{\text{n}}$ and replacing the coupled antenna patterns $\boldsymbol{A}$ by $\boldsymbol{S}_{10}$. Therefore, the weight vector (16) simplifies according to

$$\boldsymbol{w}^* = \boldsymbol{S}_{10}\left(\boldsymbol{S}_{10}^{\text{H}}\boldsymbol{S}_{10}\right)^{-1}\boldsymbol{c}^*. \tag{26}$$

This case shall be referred to as 'coupling neglected'. In the second scenario, the noise sources $\boldsymbol{n}_2$ shall not be taken into account in the noise covariance matrix $\boldsymbol{R}_{\text{n}}$ in Equation (13). This means the beamforming weights in Equation (16) take the form

$$\boldsymbol{w}^* = \boldsymbol{R}_{\text{n}_{13}}^{-1}\boldsymbol{A}\left(\boldsymbol{A}^{\text{H}}\boldsymbol{R}_{\text{n}_{13}}^{-1}\boldsymbol{A}\right)^{-1}\boldsymbol{c}^*, \tag{27}$$

where the noise covariance matrix $\boldsymbol{R}_{\text{n}_{13}}$ does not include the noise term with $\boldsymbol{n}_2$.

Figure 6 shows the normalised SNR versus the angle coordinate ϑ. The blue curves represent the reference scenario, while the red patterns are the cases where coupling has been neglected (Figure 6a) and the noise sources $\boldsymbol{n}_2$ have not been taken into account (Figure 6b). With the constraint vector $\boldsymbol{c}$ given in Table 1, the interferer direction at −1.75° has been suppressed by 60 dB, while the mainlobe points at the signal direction $\vartheta_0 = 0°$. However, since the interferer is 20 dB stronger than the signal, the resulting SIR is 40 dB. The values for the SNR according to Equation (20), evaluated at the mainlobe maximum $\vartheta_0 = 0°$, the SIR according to (21) and the SINR according to (22) have been summarised in Table 2. It is important to mention here that the SNR, the SIR and the SINR are frequency averages. This means that the beamforming weights have been re-computed for every frequency sample. Corresponding to the SNR patterns presented in Figure 6a, Figure 7 shows the normalised patterns in the angle-frequency domain. One can observe the same effect as on the coupling parameter shown in Figure 5, namely a ripple on the sidelobe at +4°, which is a consequence of multi-path propagation between feed array and reflector. This clearly demonstrates that any beamforming technique, using as input antenna patterns, for instance, at the centre frequency, will fail in placing 'Nulls' in directions where strong variations of the pattern over frequency occur.

From the results given in Table 2, one might conclude that omitting the noise sources $\boldsymbol{n}_2$ in the system modelling and the derivation of the beamformer is justified. However, there can be situations where the noise sources $\boldsymbol{n}_2$ indeed play a role. Looking at an entire range of relative noise powers $\sigma^2_{\boldsymbol{n}_1}/\sigma^2_{\boldsymbol{n}_3}$, say between −60 and −10 dB and a range of relative noise

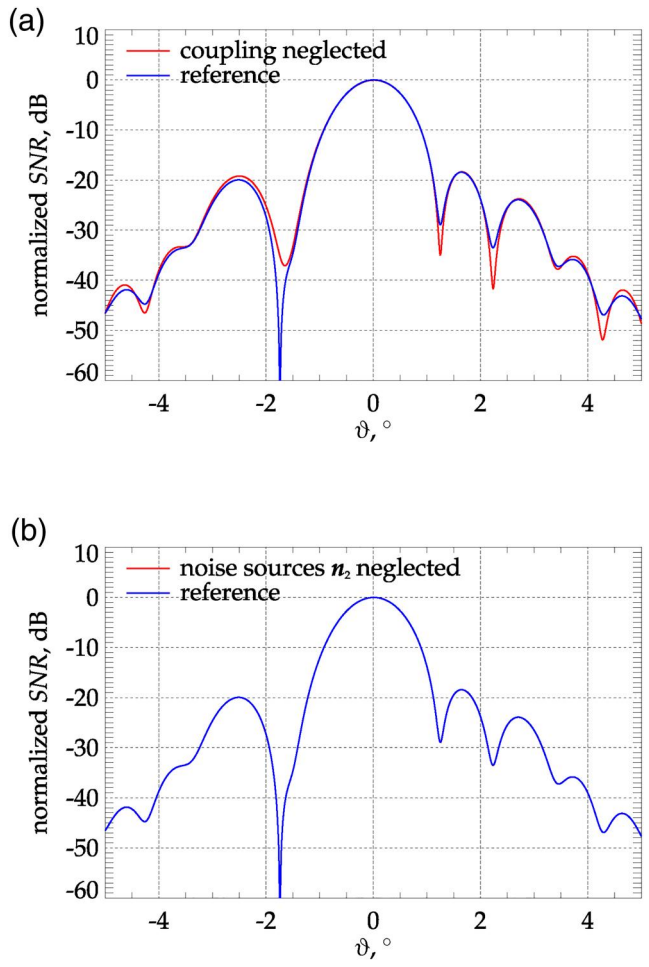

FIGURE 6 Normalised SNR patterns versus angle ϑ. In (a), the case when coupling is completely neglected in the derivation of the beamforming weights is compared with the reference case, while in (b), the case is presented when the noise sources $\boldsymbol{n}_2$ have been omitted

TABLE 2 Performance results for the two beamforming approaches in comparison to the reference case of ideal beamforming

	Reference	$\boldsymbol{n}_2$ neglected	Coupling neglected
SNR	16.70 dB	16.70 dB	16.66 dB
SIR	40.00 dB	40.00 dB	14.89 dB
SINR	16.68 dB	16.68 dB	12.68 dB

Abbreviations: SIR, signal-to-interference ratio; SINR, signal-to-interference-plus-noise ratio; SNR, signal-to-noise ratio.

powers $\sigma^2_{\boldsymbol{n}_2}/\sigma^2_{\boldsymbol{n}_3}$ between −60 and −20 dB reveals a 'bad operational regime', when the noise sources $\boldsymbol{n}_2$ are not taken into account properly in the beamforming. In Figure 8, the performance in terms of the relative SNR

$$\Delta\text{SNR} = \frac{\text{SNR}}{\text{SNR}_{\text{ref}}} \tag{28}$$

has been evaluated. Concerning the loss in interference suppression $\Delta\text{SIR} = \text{SIR}/\text{SIR}_{\text{ref}}$, it turns out that it is constant 0 dB. As a consequence, the relative SINR $\Delta\text{SINR} = \text{SINR}/\text{SINR}_{\text{ref}}$ exhibits the same behaviour and level as the ΔSNR and is therefore not plotted here. It is to be noted that according to Equation (25) and the assumed parameter values, the horizontal axis corresponds to LNA gain values G between 60 and 10 dB. The results corresponding to the parameters in

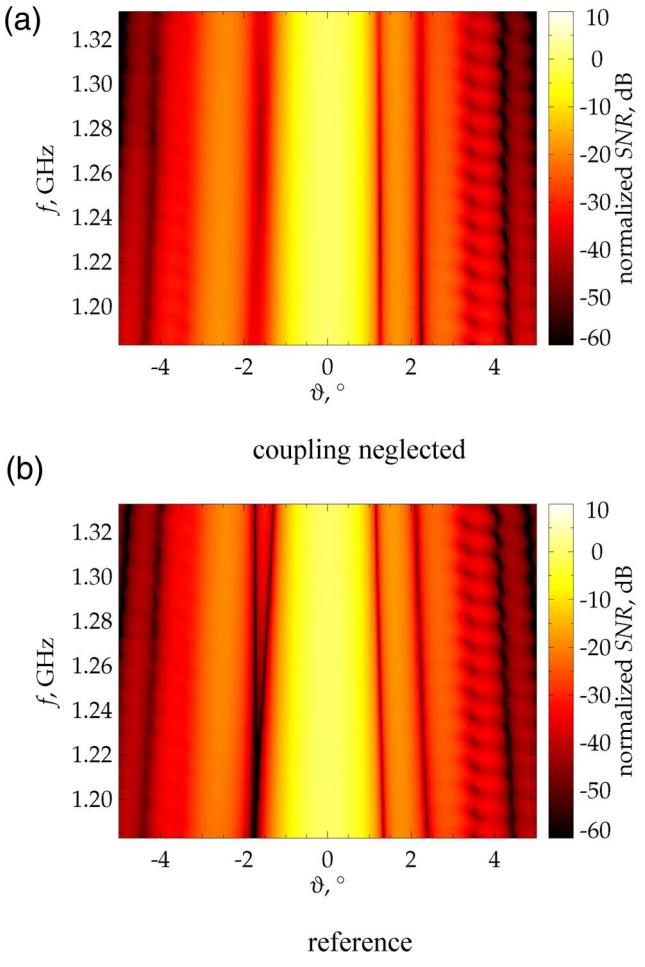

FIGURE 7 Normalised SNR patterns versus angle ϑ and frequency f for the case when coupling is neglected (a) and the reference case (b). SNR, signal-to-noise ratio

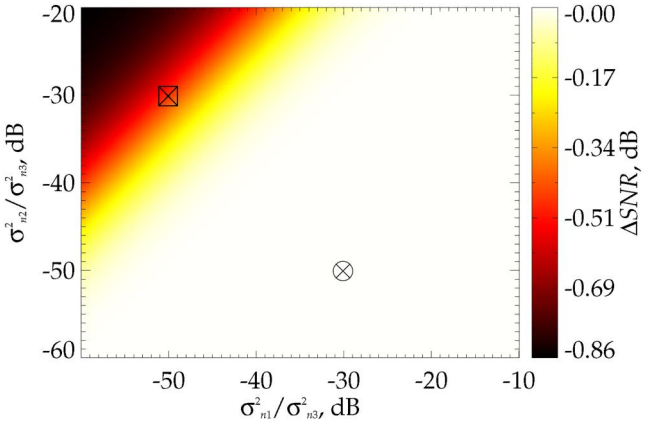

FIGURE 8 Performance in terms of the relative SNR, when the noise sources $\boldsymbol{n}_2$ are neglected during beamforming. SNR, signal-to-noise ratio

TABLE 3 Performance example in the 'bad regime' when the noise sources $\boldsymbol{n}_2$ are neglected in comparison to the reference case

	Reference	$\boldsymbol{n}_2$ neglected	Coupling neglected
SNR	27.65 dB	27.18 dB	26.86 dB
SIR	40.00 dB	40.00 dB	14.89 dB
SINR	27.41 dB	26.96 dB	14.63 dB

Note: If coupling is neglected the performance degradation gets even worse.

Abbreviations: SIR, signal-to-interference ratio; SINR, signal-to-interference-plus-noise ratio; SNR, signal-to-noise ratio.

Table 2 are marked by the ⊗-symbol and could be characterised as the 'good operational regime'. The 'bad operational regime' would be characterised by large gain factors G or small relative noise powers $\sigma^2_{\boldsymbol{n}_1}/\sigma^2_{\boldsymbol{n}_3}$, respectively, and large relative noise powers $\sigma^2_{\boldsymbol{n}_2}/\sigma^2_{\boldsymbol{n}_3}$. Here, the 'bad regime', where a loss of at least 0.1 dB occurs, is given by

$$\frac{\sigma^2_{\boldsymbol{n}_2}}{\sigma^2_{\boldsymbol{n}_1}} \gtrapprox 11 \text{ dB}. \tag{29}$$

A numerical example in the bad regime is given in Table 3 and marked by the ⊠-symbol in Figure 8. In this case, $\sigma^2_{\boldsymbol{n}_1}/\sigma^2_{\boldsymbol{n}_3}$ is −50 dB, corresponding to a gain G of 50 dB and $\sigma^2_{\boldsymbol{n}_2}/\sigma^2_{\boldsymbol{n}_3}$ is −30 dB. Correspondingly, in Figure 9 the antenna pattern is presented, where a degradation of the SNR in the mainlobe direction of 0.47 dB can be noticed.

In summary, one can assert that in the 'good operational' regime, with a numerical example given in Table 2, neglecting coupling effects in the beamforming yields a degradation in terms of the interference suppression capabilities, but no significant performance degradation when the noise sources $\boldsymbol{n}_2$ are not taken into account properly. In contrast, in the 'bad regime', represented by the example given in Table 3, an imprecise noise characterisation produces a noticeable loss in terms of the systems sensitivity.

5.1 | Interpretation of the results

In order to get more insight into the beamforming process, it is worth having a closer look at how thermal noise behaves in a coupled environment, as the one presented in Figure 1. Noise, or similarly signals, appear in the general form $\boldsymbol{Qp}$ (see Equation 8). The corresponding covariance matrix $\boldsymbol{R}_\mathrm{p}$ then takes the form $\boldsymbol{Q}\mathcal{E}\{\boldsymbol{p}\boldsymbol{p}^\mathrm{H}\}\boldsymbol{Q}^\mathrm{H}$ (compare with Equation 13). As an example from the 'bad regime', the normalised noise covariance matrices at the centre frequency for the reference case taking all noise sources into account and when the noise sources $\boldsymbol{n}_2$ are omitted, are shown in Figure 10. Interestingly, the covariances at position $(i, i+2)$ and $(i+2, i)$ seem to be stronger than those at $(i, i+1)$ and $(i+1, i)$. This may be explained by expanding $\boldsymbol{Q}\mathcal{E}\{\boldsymbol{p}\boldsymbol{p}^\mathrm{H}\}\boldsymbol{Q}^\mathrm{H}$, yielding

$$R_{\mathrm{p},ij} = \sum_k \sum_l Q_{ik} \cdot Q^*_{jl} \cdot \mathcal{E}\{p_k p^*_l\} \tag{30}$$

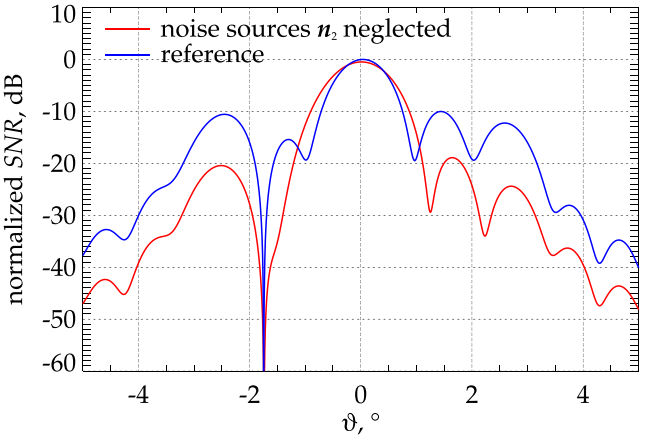

FIGURE 9 Normalised SNR patterns versus angle ϑ, when the noise sources $\boldsymbol{n}_2$ have been omitted, as example of the 'bad regime'. SNR, signal-to-noise ratio

$$= \sigma^2_\mathrm{p} \sum_k Q_{ik} \cdot Q^*_{jk}. \tag{31}$$

Here again, Gaussian independent processes p_i, with variance σ^2_p, have been assumed. In a very simple model, the individual functions Q_{ik} could represent path length delays $\tau_{ik} = r_{ik}/c$. Then, the components of the covariance matrix would take the form

$$R_{\mathrm{p},ij}(f) = \sigma^2_\mathrm{p} \sum_k \mathrm{e}^{-\mathrm{j}2\pi f \tau_{ik}} \cdot \mathrm{e}^{\mathrm{j}2\pi f \tau_{jk}}. \tag{32}$$

It is clear now that the sum of complex phasors can produce destructive superposition yielding weaker coupling even for channels that are more closely spaced.

6 | DISCUSSION AND CONCLUSION

A network-theoretical description of a multi-channel receiver system with digital beamforming is presented. The degree of generalisation is new, where noise sources have been placed at every port. Introducing this conceptual symmetry allows writing each receiver block by a single type of equation, for example, (3). Further generalisation of these equations, to model dual-polarised receiver systems, has been given in the appendix. It is important to mention that the approach developed here can be applied to other multi-channel systems. The L-band case presented here serves just as an example.

A large amount of effort has been put in the design and simulation of the feed array, using patch elements, in conjunction with the reflector. This allowed us to include realistic scattering and coupling parameters into the system equations. The S-parameters and the antenna patterns of the array-fed reflector exhibit characteristic ripples, which are related to multipath-interaction between the feed array and the reflector.

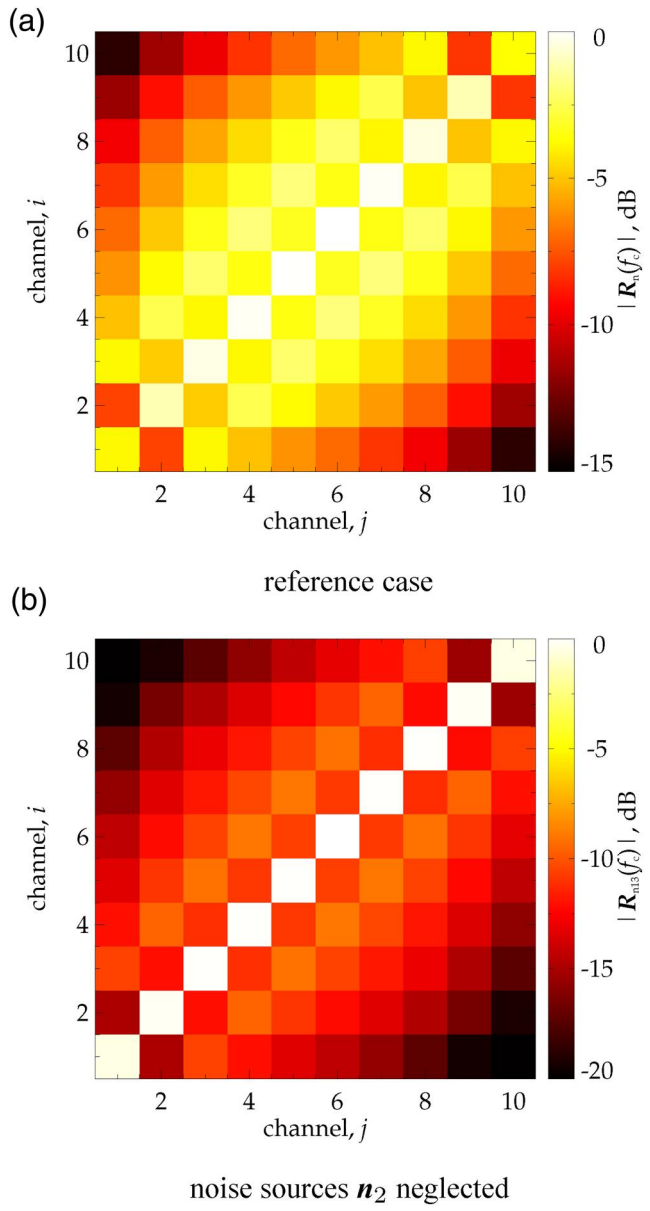

FIGURE 10 Normalised magnitude of the elements of the noise covariance matrix plotted at the centre frequency for the reference case (a) and the case when the noise sources $\boldsymbol{n}_2$ are neglected. These covariance matrices belong to the 'bad regime' with the corresponding performance given in Table 3

Many modern remote sensing systems have multi-channel architectures. This introduces new techniques for the retrieval and processing of information, since the data of the channels are individually available and can therefore be combined digitally. Here, we have investigated the performance of a null-steering technique, known as LCMV beamforming to some extent. One could have looked at other techniques, as for example, a constrained *minimum variance distortionless response* beamformer [25], where not only a single direction in the sidelobes is suppressed, but an entire domain. However, regarding their sensitivity with respect to imprecise coupling knowledge, these type of beamformers behave similarly.

The investigation shows a clear degradation of the interference rejection performance when coupling effects are not considered in the derivation of the beamforming coefficients. In our particular example with specified noise, interference and signal strength, the loss in SIR was in the order of 26 and 0.45 dB for the SINR. These performance figures could be even worse for planar array antennas, since those antennas do not benefit from the inherently low sidelobes of array-fed reflector antennas. In radio astronomy, interference relative to the signal could potentially be much stronger than assumed here.

Noise coupling in the system is a further source for performance degradation unless characterised adequately. It turned out that under certain conditions, disregarding the noise sources $\boldsymbol{n}_2$ at the input ports of the LNAs in the beamforming process can lead to a loss of sensitivity. This could happen for large amplifier gains and relatively strong noise sources $\boldsymbol{n}_2$. In this 'bad regime', SNR losses up to 0.86 dB were found (see Figure 8). For modern Earth observation radar systems, losses in this order of magnitude would not be acceptable. In contrast, the interference suppression is practically unaffected, as the numbers in Table 3 indicate. The results when the system is operated in the bad regime and when coupling is neglected have not been presented here, but it is obvious that the performance in terms of the SNR and the SIR would be even worse.

The analysis of the covariance matrix shows that there might be a chance, given a precise noise characterisation, to reduce noise coupling via an adapted feed array design. By a proper choice of the coupling path lengths, it might be possible to reduce coupling to a certain degree.

In conclusion, one might notice that the problem of coupling in multi-channel reflector antenna-based receiver systems has to be judged for each application individually. For example, for Earth observation missions, system requirements became very demanding in recent years. This drives the system design and raises the need for sophisticated radar signal processing techniques in order to reduce the susceptibility to interferences. With the approach developed here, such systems can be analysed accurately.

Currently at the German Aeropace Centre, the development of a ground-based beamforming demonstrator with reflector antenna is pushed on. This could provide more insight based on real measurements. In any case, with the increasing number of microwave systems in the future, a thorough understanding of coupling effects in multi-channel architectures seems unavoidable for their successful operation.

ORCID

Sigurd Huber https://orcid.org/0000-0001-7097-5127

REFERENCES

1. Krieger, G., et al.: The Tandem-L mission proposal: monitoring Earth's dynamics with high resolution SAR interferometry. IEEE Radar Conference (2009)

2. Moreira, A., et al.: Tandem-L: a highly innovative bistatic SAR mission for global observation of dynamic processes on the Earth's surface. IEEE Geosci. Remote Sens. Mag. 3(2), 8–23 (2015)
3. Huber, S., et al.: Tandem-L: a technical perspective on future spaceborne SAR sensors for Earth observation. IEEE Trans. Geosci. Remote Sens. 56(8), 4792–4807 (2018)
4. Warnick, K.F., et al.: High-sensitivity phased array receivers for radio astronomy. Proc. IEEE. 104(3), 607–622 (2016)
5. Winters, J.H.: Optimum combining in digital mobile radio with cochannel interferenc. IEEE Trans. Veh. Technol. 33(3), 144–155 (1984)
6. Kuehnke, L., et al.: A prototype digital beamforming antenna for future satellite communications. 29th European Microwave Conference, Vol. 2, pp. 141–144. (1999)
7. Montesinos, J., Besson, O., De Tournemine, C.L.: Adaptive beamforming for large arrays in satellite communications systems with dispersed coverage. IET Commun. 5(3), 350–361 (2011)
8. Huber, S., et al.: Advanced spaceborne SAR systems with array-fed reflector antennas. IEEE Radar Conference (RadarCon). pp. 0253–0258. (2015)
9. Krieger, G., et al.: CEBRAS: cross elevation beam range ambiguity suppression for high-resolution wide-swath and MIMO-SAR imaging. IEEE International Geoscience and Remote sensing Symposium. pp. 196–199. (2015)
10. Krieger, G., et al.: In-orbit relative amplitude and Phase Antenna pattern Calibration for Tandem-L. 12th European Conference on Synthetic aperture Radar. (2018)
11. Svantesson, T., Ranheim, A.: Mutual coupling effects on the capacity of multielement antenna systems. IEEE International Conference on Acoustics, Speech, and Signal Processing. Proceedings (Cat. No.01CH37221). 4, 2485–2488 (2001)
12. Janaswamy, R.: Effect of element mutual coupling on the capacity of fixed length linear arrays. IEEE Antennas Wirel. Propag. Lett. 1, 157–160 (2002)
13. Chen, X., Zhang, S., Li, Q.: A review of mutual coupling in MIMO systems. IEEE Access. 6, 24706–24719 (2018)
14. Li, A., Masouros, C., Sellathurai, M.: Analog-digital beamforming in the MU-MISO downlink by use of tunable antenna loads. IEEE Trans. Veh. Technol. 67(4), 3114–3129 (2018)
15. Wallace, J.W., Jensen, M.A.: Mutual coupling in MIMO wireless systems: a rigorous network theory analysis. IEEE Trans. Wirel. Commun. 3(4), 1317–1325 (2004)
16. Masa-Campos, J.L., et al.: Coupling characterisation and compensation model for antenna arrays. J. Microw. Optoelectron. Electromagn. Appl. 4(2), 95–110 (2005)
17. Maaskant, R., Woestenburg, E.E.M.: Applying the active antenna impedance to achieve noise match in receiving array antennas. IEEE Antennas and Propagation Society International Symposium. pp. 5889–5892. (2007)
18. Kerns, D.M.: Plane-wave scattering-matrix theory of antennas and antenna-antenna interactions: Formulation and applications. J. Res. Natl. Bur. Stand. 80B(1), 5–51 (1976)
19. Lewis, R.L.: Spherical-wave source-scattering matrix analysis of antennas and antenna-antenna interactions. Technical Note. National Institute of Standards and Technology (1995)
20. Shore, R., Yaghjin, A.D.: Scattering-matrix analysis of linear periodic arrays of short electric dipoles. Technical Report. Air Force Research Laboratory (2004)
21. Wedge, S.W., Rutledge, D.B.: Wave techniques for noise modelling and measurement. IEEE Trans. Microw. Theor. Tech. 40(11), 2004–2012 (1992)
22. Van Trees, H.L.: Optimum Array Processing. John Wiley & Sons, Inc, New York, NY (2002)
23. Wedge, S.W., Rutledge, D.B.: Noise waves and passive linear multiports. IEEE Microw. Guid. Wave Lett. 1(5), 117–119 (1991)
24. Randa, J.: Noise characterisation of multiport amplifiers. IEEE Trans. Microw. Theor. Tech. 49(10), 1757–1763 (2001)
25. Liu, J., et al.: Adaptive beamforming with sidelobe control: a second-order cone programing approach. IEEE Signal Process Lett. 10(11), 331–334 (2003)

How to cite this article: Huber, S., et al.: Coupling effects in array-fed reflector antennas with digital beamforming. IET Microw. Antennas Propag. 15(12), 1594–1604 (2021). https://doi.org/10.1049/mia2.12174

APPENDIX

A further generalisation of a multi-channel receiver system, described by Equations 3–5 allows describing the so-called polarimetric systems. In this case, the individual radiators are dual-polarised antenna elements. A block diagram of such an architecture is presented below, where 'v' stands for vertical polarisation and 'h' refers to the horizontal polarisation (Figure A1). For each polarisation, an individual beam, denoted by the signals $u_{\mathrm{DBF,v}}$ and $u_{\mathrm{DBF,h}}$, respectively, will be formed. The corresponding system equations take the form

$$\begin{pmatrix} \boldsymbol{b}_0 \\ \boldsymbol{b}_{\mathrm{v1}} \\ \boldsymbol{b}_{\mathrm{h1}} \end{pmatrix} = \begin{pmatrix} \boldsymbol{S}_{00} & \boldsymbol{S}_{0\mathrm{v1}} & \boldsymbol{S}_{0\mathrm{h1}} \\ \boldsymbol{S}_{\mathrm{v10}} & \boldsymbol{S}_{\mathrm{v1v1}} & \boldsymbol{S}_{\mathrm{v1h1}} \\ \boldsymbol{S}_{\mathrm{h10}} & \boldsymbol{S}_{\mathrm{h1v1}} & \boldsymbol{S}_{\mathrm{h1h1}} \end{pmatrix} \begin{pmatrix} \boldsymbol{a}_0 \\ \boldsymbol{a}_{\mathrm{v1}} \\ \boldsymbol{a}_{\mathrm{h1}} \end{pmatrix} + \begin{pmatrix} \boldsymbol{n}_0 \\ \boldsymbol{n}_{\mathrm{v1}} \\ \boldsymbol{n}_{\mathrm{h1}} \end{pmatrix},$$

$$\begin{pmatrix} \boldsymbol{b}_{\mathrm{v2}} \\ \boldsymbol{b}_{\mathrm{v3}} \end{pmatrix} = \begin{pmatrix} \boldsymbol{S}_{\mathrm{v22}} & \boldsymbol{S}_{\mathrm{v23}} \\ \boldsymbol{S}_{\mathrm{v32}} & \boldsymbol{S}_{\mathrm{v33}} \end{pmatrix} \begin{pmatrix} \boldsymbol{a}_{\mathrm{v2}} \\ \boldsymbol{a}_{\mathrm{v3}} \end{pmatrix} + \begin{pmatrix} \boldsymbol{n}_{\mathrm{v2}} \\ \boldsymbol{n}_{\mathrm{v3}} \end{pmatrix},$$

$$\begin{pmatrix} \boldsymbol{b}_{\mathrm{h2}} \\ \boldsymbol{b}_{\mathrm{h3}} \end{pmatrix} = \begin{pmatrix} \boldsymbol{S}_{\mathrm{h22}} & \boldsymbol{S}_{\mathrm{h23}} \\ \boldsymbol{S}_{\mathrm{h32}} & \boldsymbol{S}_{\mathrm{h33}} \end{pmatrix} \begin{pmatrix} \boldsymbol{a}_{\mathrm{h2}} \\ \boldsymbol{a}_{\mathrm{h3}} \end{pmatrix} + \begin{pmatrix} \boldsymbol{n}_{\mathrm{h2}} \\ \boldsymbol{n}_{\mathrm{h3}} \end{pmatrix},$$

$$\boldsymbol{S}_{0\mathrm{v1}} = \boldsymbol{S}_{0\mathrm{h1}} \approx \boldsymbol{0},$$

$$\boldsymbol{b}_{\mathrm{v1}} = \boldsymbol{a}_{\mathrm{v2}}, \quad \boldsymbol{b}_{\mathrm{v2}} = \boldsymbol{a}_{\mathrm{v1}},$$

$$\boldsymbol{b}_{\mathrm{v3}} = \boldsymbol{a}_{\mathrm{v4}}, \quad \boldsymbol{b}_{\mathrm{v4}} = \boldsymbol{a}_{\mathrm{v3}} \approx \boldsymbol{0},$$

$$\boldsymbol{b}_{\mathrm{h1}} = \boldsymbol{a}_{\mathrm{h2}}, \quad \boldsymbol{b}_{\mathrm{h2}} = \boldsymbol{a}_{\mathrm{h1}},$$

$$\boldsymbol{b}_{\mathrm{h3}} = \boldsymbol{a}_{\mathrm{h4}}, \quad \boldsymbol{b}_{\mathrm{h4}} = \boldsymbol{a}_{\mathrm{h3}} \approx \boldsymbol{0}$$

and can be reduced to

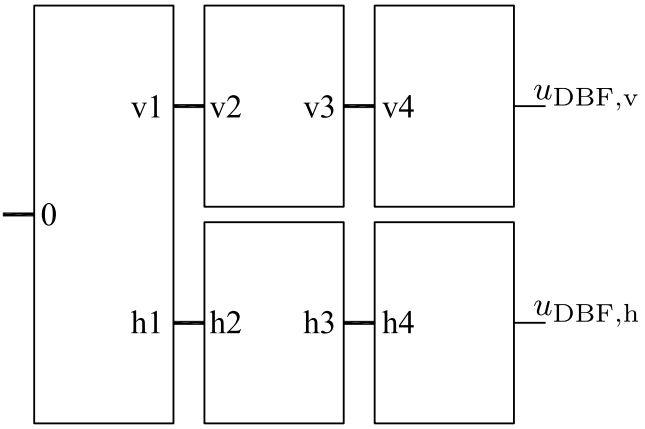

FIGURE A1 Block diagram of a dual-polarised multi-channel receiver system

$$\begin{aligned} \boldsymbol{b}_{\mathrm{v2}} &= \boldsymbol{S}_{\mathrm{v22}}(\boldsymbol{S}_{\mathrm{v10}}\boldsymbol{a}_0 + \boldsymbol{S}_{\mathrm{v1v1}}\boldsymbol{b}_{\mathrm{v2}} + \boldsymbol{S}_{\mathrm{v1h1}}\boldsymbol{b}_{\mathrm{h2}} + \boldsymbol{n}_{\mathrm{v1}}) + \boldsymbol{n}_{\mathrm{v2}} \\ \boldsymbol{a}_{\mathrm{v4}} &= \boldsymbol{S}_{\mathrm{v32}}(\boldsymbol{S}_{\mathrm{v10}}\boldsymbol{a}_0 + \boldsymbol{S}_{\mathrm{v1v1}}\boldsymbol{b}_{\mathrm{v2}} + \boldsymbol{S}_{\mathrm{v1h1}}\boldsymbol{b}_{\mathrm{h2}} + \boldsymbol{n}_{\mathrm{v1}}) + \boldsymbol{n}_{\mathrm{v3}} \\ \boldsymbol{b}_{\mathrm{h2}} &= \boldsymbol{S}_{\mathrm{h22}}(\boldsymbol{S}_{\mathrm{h10}}\boldsymbol{a}_0 + \boldsymbol{S}_{\mathrm{h1v1}}\boldsymbol{b}_{\mathrm{v2}} + \boldsymbol{S}_{\mathrm{h1h1}}\boldsymbol{b}_{\mathrm{h2}} + \boldsymbol{n}_{\mathrm{h1}}) + \boldsymbol{n}_{\mathrm{h2}} \\ \boldsymbol{a}_{\mathrm{h4}} &= \boldsymbol{S}_{\mathrm{h32}}(\boldsymbol{S}_{\mathrm{h10}}\boldsymbol{a}_0 + \boldsymbol{S}_{\mathrm{h1v1}}\boldsymbol{b}_{\mathrm{v2}} + \boldsymbol{S}_{\mathrm{h1h1}}\boldsymbol{b}_{\mathrm{h2}} + \boldsymbol{n}_{\mathrm{h1}}) + \boldsymbol{n}_{\mathrm{h3}} \end{aligned}$$

From these equations, $\boldsymbol{b}_{\mathrm{v2}}$ and $\boldsymbol{b}_{\mathrm{h2}}$ can be eliminated in order to arrive at two equations for the beamformer input $\boldsymbol{a}_{\mathrm{v4}}$ and $\boldsymbol{a}_{\mathrm{h4}}$ depending only on the scattering matrices and the noise terms, similar to Equation (8). One may notice, if a dual-polarised antenna does not exhibit coupling between the polarisation channels, meaning that $\boldsymbol{S}_{\mathrm{v1h1}} = \boldsymbol{S}_{\mathrm{h1v1}} = \boldsymbol{0}$, then these equations are identical to (6) and (7) for their respective polarisation (vertical or horizontal).